Cancer Research

Oncogenic MYC Induces the Impaired Ribosome Biogenesis Checkpoint and Stabilizes p53 Independent of Increased Ribosome Content

Carmen Morcelle[1], Sandra Menoyo[1], Francisco D. Morón-Duran[1], Albert Tauler[1,2], Sara C. Kozma[1], George Thomas[1,3], and Antonio Gentilella[1,2]

Abstract

The role of MYC in regulating p53 stability as a function of increased ribosome biogenesis is controversial. On the one hand, it was suggested that MYC drives the overexpression of ribosomal proteins (RP)L5 and RPL11, which bind and inhibit HDM2, stabilizing p53. On the other, it has been proposed that increased ribosome biogenesis leads the consumption of RPL5/RPL11 into nascent ribosomes, reducing p53 levels and enhancing tumorigenesis. Here, we show that the components that make up the recently described impaired ribosome biogenesis checkpoint (IRBC) complex, RPL5, RPL11, and *5S* rRNA, are reduced following *MYC* silencing. This leads to a rapid reduction in p53 protein half-life in an HDM2-dependent manner. In contrast, MYC induction leads to increased ribosome biogenesis and p53 protein stabilization. Unexpectedly, there is no change in free RPL5/RPL11 levels, but there is a striking increase in IRBC complex bound to HDM2. Our data support a cell-intrinsic tumor-suppressor response to MYC expression, which is presently being exploited to treat cancer.

Significance: Oncogenic MYC induces the impaired ribosome biogenesis checkpoint, which could be potentially targeted for cancer treatment.

Introduction

In a proliferating cell, the proto-oncogene *MYC* drives genome-wide transcription, particularly of those genes involved in cell-cycle progression (1, 2). Among the chief functions fulfilled by MYC in cell-cycle progression is the coordinate production of the molecular components that generate nascent ribosomes, needed for increased protein synthetic capacity in a rapidly growing cell (2). Importantly, this observation has led to the finding that oncogenic MYC-driven tumors are addicted to the hyperactivation of ribosome biogenesis (3), which may serve as an Achilles' heel for the treatment of such tumors (4). It is generally accepted that MYC coordinates nascent ribosome biogenesis through the three RNA polymerases (Pol I-III; ref. 2). However, unlike in yeast, where the transcription of rRNA and ribosomal protein (RP) genes is tightly coordinated (5), the production of RPs in higher eukaryotes appears to be largely regulated at the translational level, as first demonstrated during *Xenopus laevis* development (6). Moreover, this response is controlled through a 5′-terminal oligopyrimidine (5′TOP) sequence, residing at the transcriptional start site of RP genes (7). It is suggested that the evolution of this translational control mechanism coincided with the rise of metazoans, to more rapidly provide RPs in specific tissues (8).

The biogenesis of ribosomes is one of the most energy-consuming cellular processes and is largely confined to the nucleolus (2). In addition to the rRNAs and RPs, the production of the mature 40S and 60S ribosomal subunits involves a large number of extra ribosomal molecules including small nucleolar RNAs, as well as proteins required for rRNA processing, import of RPs into the nucleus, ribosome assembly, and their nucleolar-nuclear export to the cytoplasm (2). Perturbation of ribosome biogenesis induces the stabilization of p53, leading to cell-cycle arrest and either senescence or cell death (9). Although impaired ribosome biogenesis and the stabilization of p53 were initially attributed to nucleolar disruption (10), we and others showed this not to be the case (11, 12). Instead it was found to be mediated by an active mechanism (11), the binding and inhibition of HDM2 by a pre-ribosomal complex composed of RPL5, RPL11, and *5S* rRNA (13, 14), which we recently termed the impaired ribosome biogenesis checkpoint (IRBC; refs. 2, 9).

Critically, RPL11 and RPL5 have been also implicated in deterring *Eμ-Myc*–mediated tumorigenesis (15). Macias and colleagues showed that when a cancer-associated single point mutation within the zinc-finger domain of HDM2, C305P, which abolishes its binding to RPL5 and RPL11, but not ARF (CDKN2A), was introduced into the wild-type locus of the mouse *Mdm2* gene, such mice succumbed much more rapidly to B-cell lymphoma than control mice (15). This led to the suggestion that in such

[1]Laboratory of Cancer Metabolism, ONCOBELL Program, Bellvitge Biomedical Research Institute (IDIBELL), Barcelona, Spain. [2]Department of Biochemistry and Physiology, Faculty of Pharmacy, University of Barcelona, Barcelona, Spain. [3]Physiological Sciences Department, Faculty of Medicine and Health Science, University of Barcelona, Barcelona, Spain.

Note: Supplementary data for this article are available at Cancer Research Online (http://cancerres.aacrjournals.org/).

C. Morcelle, S. Menoyo, and F.D. Morón-Duran contributed equally to this article.

Current address for C. Morcelle: Molecular and Cell Biology Laboratory, Institutes of Biomedical Sciences, Shanghai Medical College, Shanghai, China.

Corresponding Authors: George Thomas and Antonio Gentilella, ICO/IDIBELL, Hospital Duran i Reynals Gran Via de l'Hospitalet, 19908908 Hospitalet de Llobregat, Barcelona 08908, Spain. Phone: 34932607099; Fax: 34932607782; E-mail: gthomas@idibell.cat; agentilella@idibell.cat

Cancer Res 2019;79:4348–59

doi: 10.1158/0008-5472.CAN-18-2718

tumors, RPL11 and RPL5 are overexpressed, acting to stabilize p53 and suppress MYC oncogenic potential (15). However, in parallel, others have proposed that mitogens and oncogenes, including *MYC*, by increasing rRNA synthesis, serve to drive the consumption of RPL5 and RPL11 into nascent ribosomes, such that in a proliferating cell, this would release basal inhibition of HDM2, leading to p53 protein degradation and the potential for increased tumorigenesis (16–18). Moreover, in neither of these seemingly conflicting models has the role of the IRBC complex been investigated.

Given that MYC expression is found increased or deregulated in over 70% of human tumors (19), it is important to understand the underlying cellular mechanisms responsible for mediating the cell's response to potential oncogenic threats (20). Here, we have largely focused on the role of ribosome biogenesis in colorectal cancer cell lines, as almost all sporadic colorectal cancers have elevated or deregulated levels of MYC (21). We first determined whether the mechanisms by which MYC controls global rRNA and RP production are affected in a similar or distinct manner, particularly with respect to RPL5, RPL11, and *5S* rRNA. Next, we asked to what extent lowering MYC levels affects cell-cycle progression and *p53* mRNA and protein levels and whether the IRBC complex plays a role regulating this response. In turn, we asked if the induction of MYC affects p53 protein levels and the function of the IRBC complex in this setting. Together, our findings suggest that through an active tumor cell–intrinsic mechanism, the *MYC* oncogene product is sensed, leading to the activation of the IRBC independently of increased ribosome numbers, which inhibits HDM2 and stabilizes p53.

Materials and Methods

Cell culture and reagents

RKO and HCT116 colorectal cancer cell lines were obtained from the ATCC and maintained in DMEM (Thermo Fisher Scientific) supplemented with 10% heat-inactivated FBS (Sigma-Aldrich). For all studies, cells were incubated at 37°C, 5% CO2, and 90% to 95% of relative humidity. For specified studies, ActD (BioVision Technologies) was used (5 ng/mL, 6 hours), and MG-132 (Sigma-Aldrich) and cycloheximide (Sigma-Aldrich) were used (10 μmol/L and 71.1 mmol/L respectively, for the indicated times). U2OS cells stably transfected with a doxycycline-inducible two-vector system encoding human *MYC* gene were kindly provided by M. Eilers (University of Würzburg, Würzburg, Germany; ref. 22). Induction of MYC expression was obtained by addition of doxycycline (1 μg/mL for the indicated time).

Transfections

siRNA transfections were performed in Opti-MEM medium (Life Technologies) using Lipofectamine RNA-iMAX (Life Technologies), following the manufacturer's instructions. Unless otherwise indicated, transfections were performed for 48 hours, with 50 nmol/L siRNA. The following siRNAs were used: nonsilencing (NS) control (GCAUCAGUGUCACGUAAUA) was from Sigma-Aldrich, siMYC was from Santa Cruz Biotechnology (sc-44248), siMYCa was from QIAGEN (SI02662611), and sip53 and siHDM2 were custom-ordered from Sigma (sip53GCAUCUUAUCCGAGUGGAA; and siHDM2, AACCUGAAAUUUAUUCACAUA).

Total cellular proteins extraction and Western blot analyses

Total protein extraction and SDS-PAGE were performed as previously described (11, 13). Briefly, cells grown in either 6 or 10-cm dishes were washed twice with ice-cold PBS, scraped, and lysed on ice in extraction buffer [50 mmol/L Tris-HCl (pH 8), 250 mmol/L NaCl, 1% Triton X-100, 0.25% sodium deoxycholate, 0.05% SDS, 1 mmol/L dithiothreitol (DTT), and protease inhibitors cocktail (Sigma-Aldrich)]. Lysates were cleared by centrifugation and quantified by Bradford protein assay (Bio-Rad) following the manufacturer's instructions. Primary antibodies used for Western blotting were: anti-MYC (Y69; Abcam), anti-HDM2 (SMP14; Santa Cruz Biotechnology, 2A10; Abcam), anti-p53 (DO-1; Santa Cruz Biotechnology), anti-RPL11 (3A4A7; Invitrogen), anti-RPL5 (A303-933A; Bethyl Laboratories), anti-RPL7A (PMID:2403926), anti–β-actin (A2228; Sigma-Aldrich), anti-GAPDH (2118; Cell Signaling Technology). Protein detection was performed using an enhanced chemiluminescence kit (GE Healthcare). Quantification of band intensities by densitometry was carried out using the Image J software. Absolute values obtained from the quantification of p53, MYC, and selected RPs were normalized to those of either endogenous β-actin or GAPDH. Relative values in depletion experiments were obtained by setting the NS siRNA (siNS) values to 1. Relative values in time course experiments involving cycloheximide and MG-132 treatments were obtained by setting the time point 0 values to 1.

mRNA and rRNA analyses

Total RNA was extracted from treated cells in culture (grown in 6 cm dishes), using TRIzol (Invitrogen) as recommended by manufacturer and as it has been recently described (23). RNA was resuspended in DEPC-treated water and quantified using NanoDrop 1000 spectrophotometer (Thermo Fisher Scientific). Aliquots of RNA (2–5 μg) were treated to remove DNA using DNAse I (Sigma-Aldrich) following the manufacturer's instructions. Note that 1 μg of total DNAse I–treated RNA was reverse transcribed. Gene expression was normalized to the endogenous *β-actin* mRNA. For the analysis of mRNA across polysome profiles, 10^6 RKO cells were plated in 100 mm dishes, transfected with the indicated siRNA for 48 hours, and processed. Protein concentrations were determined by BCA assay, and 500 mg of lysate were loaded on 10% to 50% sucrose linear gradients. Gradients were centrifuged on a SW40 rotor and then they were analyzed on a BIOCOMP gradient station and collected in 12 fractions ranging from light to heavy sucrose. To each fraction, 1 ng of *firefly luciferase* mRNA was added, followed by phenol–chloroform extraction and precipitation with isopropanol. Purified RNAs from each fraction were reverse-transcribed and subjected to qPCR. mRNA quantification was normalized to *firefly luciferase* mRNA.

Immunoprecipitations

Cells grown in 15 cm dishes were lysed on ice in immunoprecipitation lysis buffer [50 mmol/L Tris HCl (pH 7.5), 150 mmol/L KCl, 5 mmol/L $MgCl_2$, 1 mmol/L EGTA, 1 mmol/L DTT, 10% glycerol, 0.8% NP-40, PMSF 1 mmol/L, 100 U/mL RNaseout inhibitor (Invitrogen), and complete EDTA-free Protease Inhibitor cocktail (Roche)] and subjected to immunoprecipitation, largely as previously described (13). In brief, ribosomes were pelleted by ultracentrifugation at 200,000 × *g* at 4°C for 2 hours. Immunoprecipitations were obtained from equivalent amounts

of protein incubated at 4°C overnight with rotation with either rabbit polyclonal anti-RPL5 (A303-933A; Bethyl Laboratories) or normal rabbit IgG (sc-2027; Santa Cruz Biotechnology) added to a final sample concentration of 4 μg/mg. Note that 20 μL of PureProteomeTM Protein A/G Mix Magnetic Beads (Merck), handled following the manufacturer's instruction, were added to each sample and mixed by rotation at 4°C for 2 hours. Supernatants were discarded and beads were resuspended in either protein loading buffer for Western blot analysis or TRIzol reagent (Invitrogen) together with a spike of *firefly luciferase* mRNA, to recover immunoprecipitated RNA for *5S* rRNA qRT-PCR analysis, as described above. All primers were used for qRT-PCR analyses (Supplementary Table S1).

Cell-cycle analysis

Treated and control cells in culture were collected and fixed with 70% ethanol and placed at −20°C for at least 4 hours. Cells were then washed with ice-cold PBS supplemented with 0.1% BSA and 5 mmol/L EDTA, and centrifuged at 4°C for 5 minutes at 428 × *g*. Supernatant was discarded, and the cellular pellet was resuspended in a propidium iodide (PI) staining solution [PBS, 0.1% NP-40, 20 μg/mL RNAse A (Invitrogen), and 40 μg/mL PI (Invitrogen)] and incubated at room temperature protected from light for at least 15 minutes. Samples were analyzed using FACS Canto System.

De novo protein analysis

In brief, as we have recently described (9), before lysis, cells grown in 6 cm dishes were washed twice with methionine-free DMEM medium (Thermo Fisher Scientific) at room temperature and incubated for 15 minutes in 3 mL of methionine-free DMEM medium (Thermo Fisher Scientific) supplemented with 10% dialyzed serum (Sigma-Aldrich), pyruvate 1 mmol/L (Thermo Fisher Scientific), GlutaMAX (Thermo Fisher Scientific), L-cystine (Sigma-Aldrich), HEPES 25 mmol/L (Thermo Fisher Scientific), and equilibrated to pH 7.4 with NaOH. The media were then replaced with the same methionine-free medium, supplemented with 50 μmol/L L-azidohomoalanine (AHA; Invitrogen) for 2 hours. AHA-labeled proteins were chemically processed using the Click-iT Protein Reaction Buffer Kit (Thermo Fisher Scientific), according to the manufacturer's protocol, and the biotin–alkaline-conjugated proteins were resuspended in 1% SDS. A 20 μg aliquot of total protein was separated on SDS polyacrylamide gels, transferred to nitrocellulose membranes, stained with Streptavidin-IRDye 800CW (Li-Cor Biosciences), and then the stained membranes were scanned with the Odyssey detection system (Li-Cor Biosciences). For detection of individual proteins, 200 μg of the biotin–alkaline-conjugated proteins were diluted in 50 mmol/L Tris (pH 7.4), 150 mmol/L NaCl, 0.1% SDS supplemented with Proteases Inhibitors, and incubated for 2 hours at room temperature with Pierce streptavidin-agarose beads (Thermo Fisher Scientific). Streptavidin–biotin conjugates were washed 3 times with 500 μL of wash solution [Tris-HCl (pH 7.4) 50 mmol/L, NaCl 150 mmol/L, SDS 0.1%], resuspended in Laemmli sample buffer, resolved on 10% SDS-PAGE gels, and probed with the indicated antibodies (9).

Autoradiographic analysis of proteins and rRNA

For the analysis of newly synthesized proteins, cells were pulse-labeled with ^{3}H-leucine or AHA as described above, whereas for newly synthesized RNA, they were pulse-labeled with ^{3}H-uridine, and then each sample was processed as recently described (9).

Crystal violet staining

Cells plated in 6-well plates were allowed to adhere overnight. After the indicated treatment, cells were washed twice with room temperature PBS and incubated for 10 minutes at room temperature with 750 μL of crystal violet solution (Sigma-Aldrich). The crystal violet solution was then discarded, and cells were rinsed with water. Subsequent 10- to 15-minute washes with water were performed until residual noncellular staining was eliminated. Stained cells were lysed by adding 1.5 mL of 2% SDS per well on an orbital shaker until the sample was completely dissolved. Absorbance at 540 nm was measured in a microplate reader. Experimental conditions were performed in triplicate.

Statistical analysis

Results are presented as mean ± SE., for $n = 2$–3. Experimental datasets were compared by a two-sampled, two-tailed Student *t* tests. Values of *, $P < 0.05$; **, $P < 0.005$; and ***, $P < 0.0005$ were considered statistically significant.

Results

MYC depletion inhibits rRNA synthesis and global translation

In cell lines derived from human colorectal cancer, it is known that overexpressed or deregulated MYC drives increased rates of ribosome biogenesis, leading to increased levels of global protein synthesis (2). To determine the extent to which MYC affects these responses, we transfected either a siNS or two distinct *MYC* siRNAs (siMYC and siMYCa) in RKO cells, a poorly differentiated aggressive colorectal cancer cell line (24). Cells treated with the *MYC*-specific siRNAs, as compared with those treated with the siNS, show a strong decrease in *MYC* mRNA and MYC protein levels (Fig. 1A and B, respectively). To determine the effects of loss of MYC on ribosome biogenesis, we measured nascent rRNA levels, by pulse labeling siRNA-treated RKO cells with ^{3}H-uridine (11, 13). Analysis of an agarose gel loaded with equal amounts of total cellular rRNA, as detected by ethidium bromide (EB) staining (Fig. 1C, left), shows that MYC depletion had a profound effect on the rate of incorporation of ^{3}H-uridine into the newly synthesized *18S* and *28S* rRNA, when compared with siNS-treated cells (Fig. 1C, right). This was also the case for *5S*, *5.8S* rRNAs, and tRNAs, as analyzed on polyacrylamide gels (Fig. 1D). Similar results were also obtained in HCT116 cells (Supplementary Fig. S1A and S1B). Moreover, the effects on ribosome biogenesis are paralleled by an approximately 50% decrease in global protein synthesis, as measured by the incorporation of ^{3}H-leucine into nascent protein in RKO cells (Fig. 1E). The findings are consistent with MYC's role as major driver of ribosome biogenesis and protein synthesis.

MYC regulates the expression of RPL5 and RPL11 at the mRNA level

Given the potential importance of nascent RPL5 and RPL11 in mediating the IRBC in response to MYC, we analyzed the effects of MYC depletion on the transcription and translation of *RP* mRNAs. The results show that depletion of MYC, as compared with siNS-treated cells, led to a decrease in the relative amounts of a number of *RP* mRNAs analyzed, including *RPL5*, *RPL11*, *RPL7a*, and *RPS19*, as compared with that of *β-actin* mRNA (Fig. 2A). In

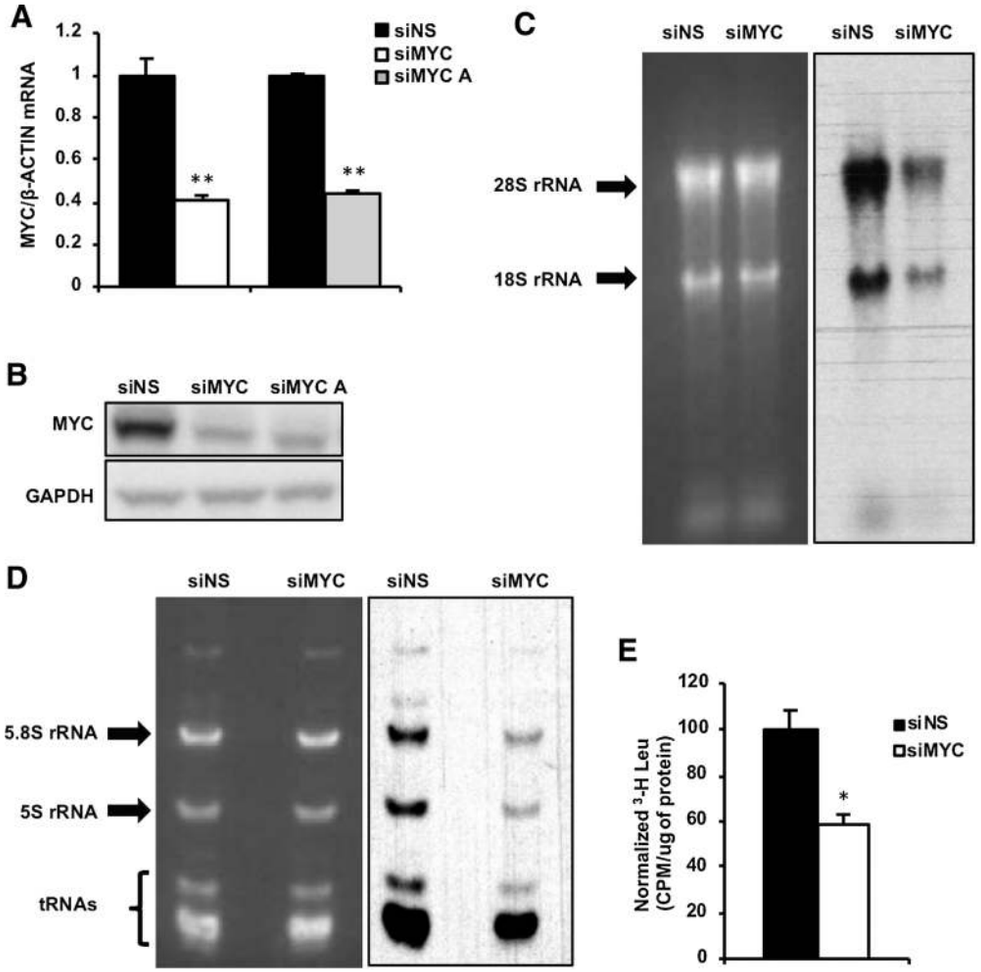

Figure 1.

Effects of MYC depletion on rRNA and protein synthesis. **A,** RKO cells were transfected with 50 nmol/L of either siNS, siMYC, or siMYCa for 48 hours, and *MYC* mRNA levels were determined by qRT-PCR relative to *β-actin* mRNA levels (data are mean ± SEM; $n = 3$). **B,** RKO cells were transfected with siNS, siMYC, or siMYCa as in **A,** and whole-cell lysates were subjected to Western blot analysis with indicated antibodies, with GAPDH serving as a loading control. **C,** EB-stained agarose gel (left) and autoradiogram (right) to detect *18S* and *28S* rRNA from RKO cells treated with siNS or siMYC as in **A**, labeled for 1 hour with ^{3}H-uridine and chased for 4 hours in nonlabeled uridine-containing medium. **D,** EB-stained TBE-urea polyacrylamide gel (left) and autoradiogram (right) to detect *5S* rRNA, *5.8S* rRNA, and tRNAs in RKO cells transfected with siNS or siMYC as in **B**. **E,** Quantification of ^{3}H-leucine incorporation in total cellular proteins from RKO cells treated with siNS or siMYC as in **A** (data are mean ± SEM from three different dishes. *, $P < 0.05$; **, $P < 0.005$, calculated by Student *t* test.

parallel, there appears to be little effect on the steady-state levels of their cognate RP proteins (Fig. 2B). To determine the effect of MYC depletion on nascent translation of *RPs,* we focused on RPL5. We first pulse-labeled *NS* or *MYC* siRNA–treated cells with the non-radioactive methionine analogue AHA, as we have recently described (9). Total cell extracts were then treated with biotin-conjugated alkaline, such that the nascent proteins could be detected by Streptavidin-IRDye 800CW (9). Analysis by amido-black staining shows that the amounts of total protein loaded were roughly equivalent (Fig. 2C, left). However, the newly synthesized biotinylated proteins, detected by streptavidin-IRDye800 staining (9), were largely decreased in MYC-depleted cells as compared with *NS* siRNA–treated control cells (Fig. 2C, right), consistent with the decrease in nascent protein synthesis, measured by pulse-labeling proteins with ^{3}H-leucine (Fig. 1E). When compared with GAPDH, there was an approximate 24% drop in total RPL5 protein levels in MYC-depleted cells as compared with *NS* siRNA–treated control cells (Fig. 2D, left). However, the amount of newly synthesized RPL5 pulled down by streptavidin-agarose beads was reduced by almost 70% when compared with newly synthesized GAPDH (Fig. 2D, right). The results suggest that depletion of MYC has an impact on mature RP population, which is largely due to nascent RP and rRNA synthesis (compare Fig. 2D with Fig. 1C and D).

Although the extent to which MYC depletion leads to a reduction in *RPL5* mRNA (Fig. 2A) roughly parallels that observed for global translation (Figs. 1E and 2C) and newly synthesized RPL5 protein (Fig. 2D), recent studies show that MYC induction also drives the selective expression of RP mRNAs at the translational level (25). To test this possibility, we examined equal amounts of cell protein lysates following nonionic detergent extraction, required to preserve polysomes, and analyzed the distribution

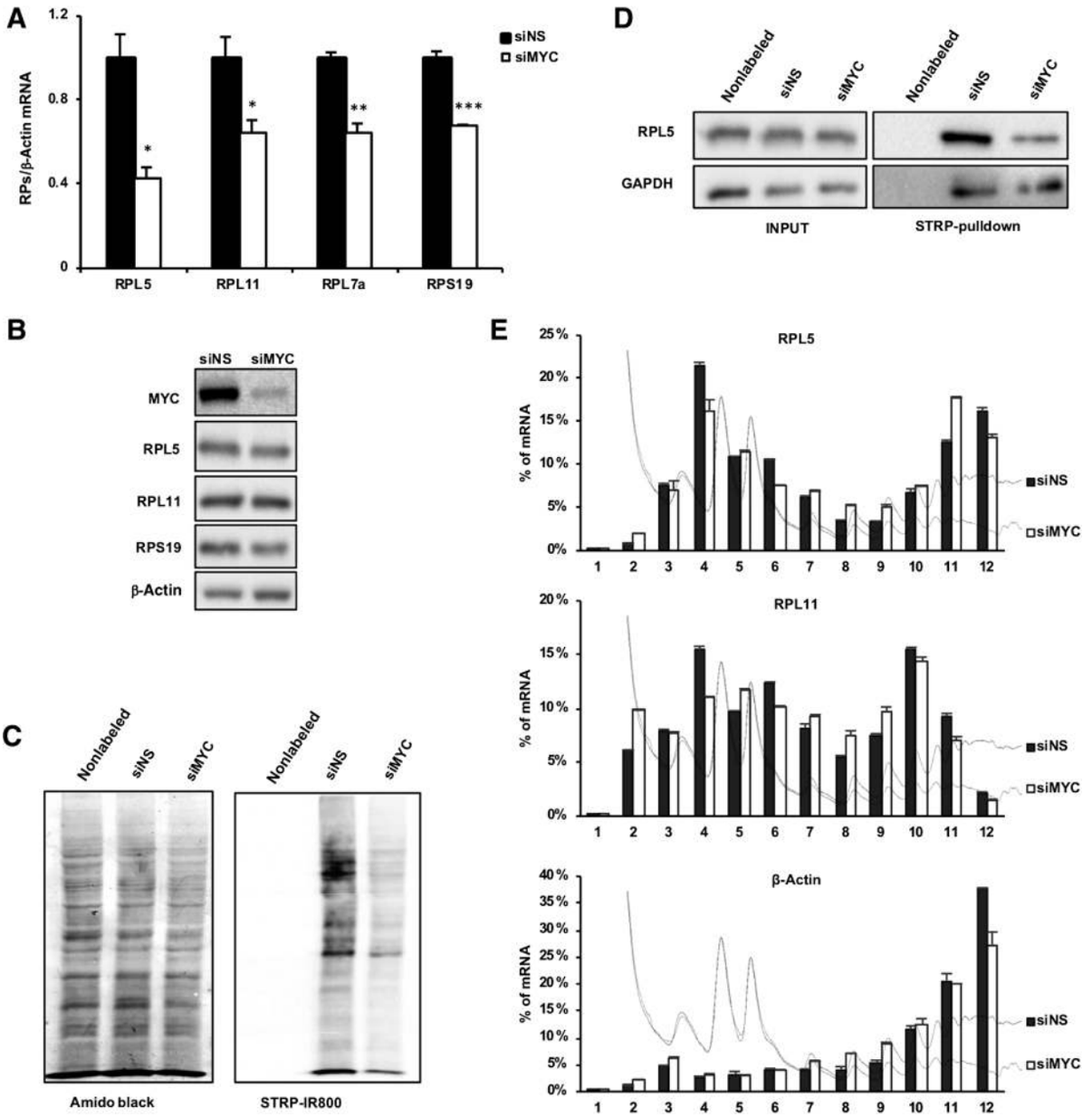

Figure 2.

Effect of MYC depletion on *RP* mRNAs and RPs. **A,** RKO cells were treated with siNS or siMYC for 48 hours, and mRNA levels of indicated RPs were determined by qRT-PCR relative to *β-actin* mRNA levels (data are mean ± SEM; $n = 3$). **B,** RKO cells were treated as in **A**, and whole-cell lysates were subjected to Western blot analysis with indicated antibodies, with β-actin protein serving as a loading control. **C,** RKO cells were treated as in **A**, and *de novo*–synthesized proteins were labeled in the alkyne–biotin Click-iT reaction. The same amount of total proteins loaded was analyzed, staining with amido black (left) or streptavidin-IRDye800 (right). **D,** The Western blot in **C** (INPUT; left) or a Western blot following streptavidin-pulldown nascent proteins from **C** (STRP-pulldown; right) was analyzed with the indicated antibodies. Quantification was performed as described in Materials and Methods. For MYC-depleted samples, the relative values of total RPL5 and AHA-labeled RPL5, as compared with those from siNS-treated samples, were 0.76 and 0.32, respectively. **E,** Total cell extracts from RKO cells treated for 48 hours with siNS (top polysome profile in each case) or siMYC (bottom polysome profile in each case) were fractionated on sucrose gradients, each spiked with *firefly luciferase* mRNA, and the distribution of indicated mRNA species was determined by RT-qPCR relative to *firefly luciferase* mRNA. *, $P < 0.05$; **, $P < 0.005$; ***, $P < 0.0005$, calculated by Student *t* test.

of *RP* mRNAs across sucrose gradients from *NS* siRNA– and *MYC* siRNA–treated cells, as we have previously described (11). Consistent with the decrease in global protein synthesis (Figs. 1E and 2C), the amount of polysomes as compared with small/nonpolysomes appears to be proportionally reduced in *MYC* versus *NS* siRNA–treated cells (Fig. 2E). In *NS* siRNA–treated cells, *RPL5* and *RPL11* mRNAs are distributed roughly equally in small/nonpolysome versus large polysome fractions of the

gradient, as measured by qRT-PCR, whereas that of *β-actin* mRNA is largely present on actively translating polysomes (Fig. 2E). In *MYC* siRNA–treated cells, *RPL5* and *RPL11* mRNAs are little changed in their proportional distribution in small/nonpolysomes versus large polysomes (Fig. 2E). Similarly, *β-actin* mRNA remains localized on actively translating polysomes. Thus, the effects of the loss of MYC on RP expression do not appear to be mediated by their selective inhibition at the translational level, but appear instead to be primarily regulated by the decreased levels of their mRNAs.

MYC depletion inhibits cell growth and suppresses p53 protein expression

Others have argued that reducing MYC levels selectively inhibits rRNA synthesis increasing the levels of free RPL5 and RPL11, blocking HDM2, and inducing p53 stabilization (17). However, we find that depletion of MYC coordinately lowers the levels of both nascent rRNAs (Fig. 1C and D) and apparently their corresponding RPs (Fig. 2D), including the components that make up the IRBC, which would be predicted to result in decreasing cell growth and p53 protein levels. Consistent with this model, we find that depleting MYC levels in RKO cells leads to a reduction in the rate of cell proliferation (Fig. 3A) and the accumulation of cells in the G_0–G_1 phases of the cycle (Fig. 3B). Similar results were obtained for HCT116 cells (Supplementary Fig. S2A and S2B). These findings are consistent with the role of MYC in driving the expression of key cell-cycle regulators required for cells to progress into S phase, including E2F1 and the cyclins. However, the decrease in ribosome biogenesis, cell proliferation, and the accumulation of cells in the G_0–G_1 phase of the cell cycle following depletion of MYC could be attributed to the stabilization of p53 (17, 18). We find, in both RKO and HCT116 cells, MYC depletion instead led to a reduction in p53 protein levels as well as those of HDM2 (Fig. 3C and Supplementary Fig. S2C, respectively). Moreover, in contrast to the findings of Brighenti and colleagues in HepG2 cells (17), we found that treatment with siMYC also led to a time-dependent reduction of p53 and HDM2 protein levels in HepG2 cells (Fig. 3D). Thus, in the absence of MYC, cells accumulate in G_0–G_1 phase of the cell cycle, cell proliferation is reduced, as is the apparent "oncogenic stress," defined by the expression of oncogenes leading to the activation of antioncogenic pathways (26), as reflected here by the apparent reduction in p53 protein levels.

Reduction of p53 protein levels is controlled at the posttranscriptional/posttranslational level

Given that p53 protein amounts are evidently decreasing following MYC depletion, it was important to determine at which step its expression was regulated. Unlike *RP* mRNAs (Fig. 2A), we found that the relative levels of *p53* mRNA, as compared with *β-actin* mRNA, were relatively unchanged following MYC depletion, in both RKO and HCT116 cells (Fig. 4A). As shown above, global protein synthesis was diminished in MYC-depleted cells (Figs. 1E and 2C). This raised the possibility that even though *p53* mRNA levels are maintained, its nascent protein levels are declining, as those of RPL5 (Fig. 2D). To test this possibility, we analyzed the AHA-pulse–labeled Western blot for newly synthesized biotinylated p53 as described above (Fig. 2C and D). As depicted

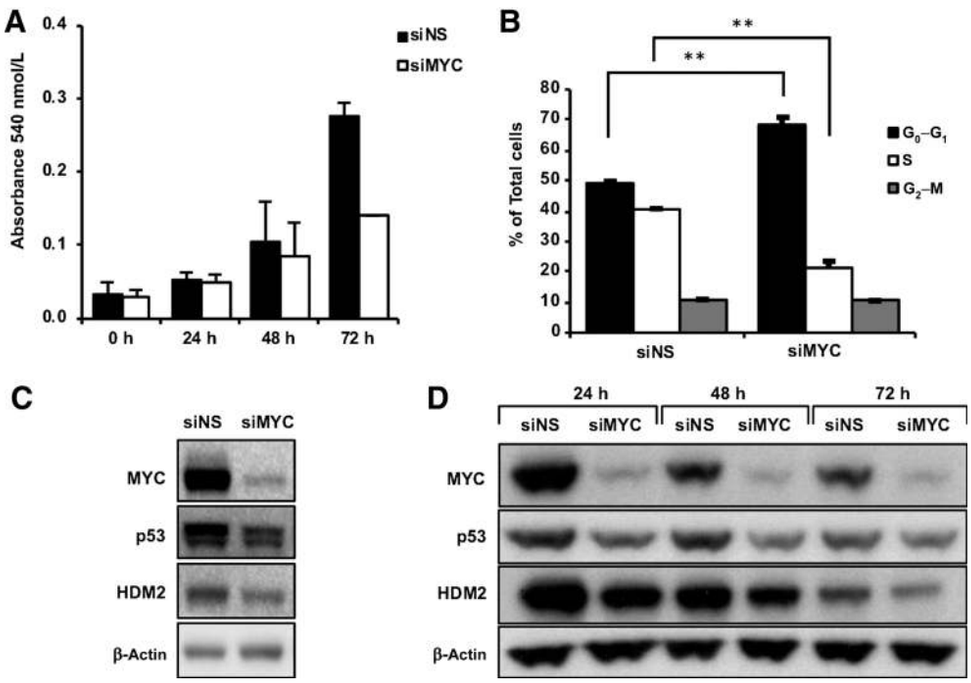

Figure 3.

Effects of MYC depletion on cell growth and p53 protein levels. **A,** RKO cells were transfected with siNS or siMYC for 24, 48, and 72 hours, and the rate of proliferation was measured by crystal violet staining (data are mean ± SEM from two independent experiments). **B,** RKO cells were treated with siNS or siMYC for 48 hours and analyzed by flow cytometry. **C,** RKO cells treated as in **B** were examined by Western blot analysis for the indicated proteins, with β-actin protein serving as a loading control. **D,** Western blot analyses of time course of p53 protein expression in siNS and siMYC-silenced HepG2 cells for the times indicated, with β-actin serving as a loading control. **, $P < 0.005$.

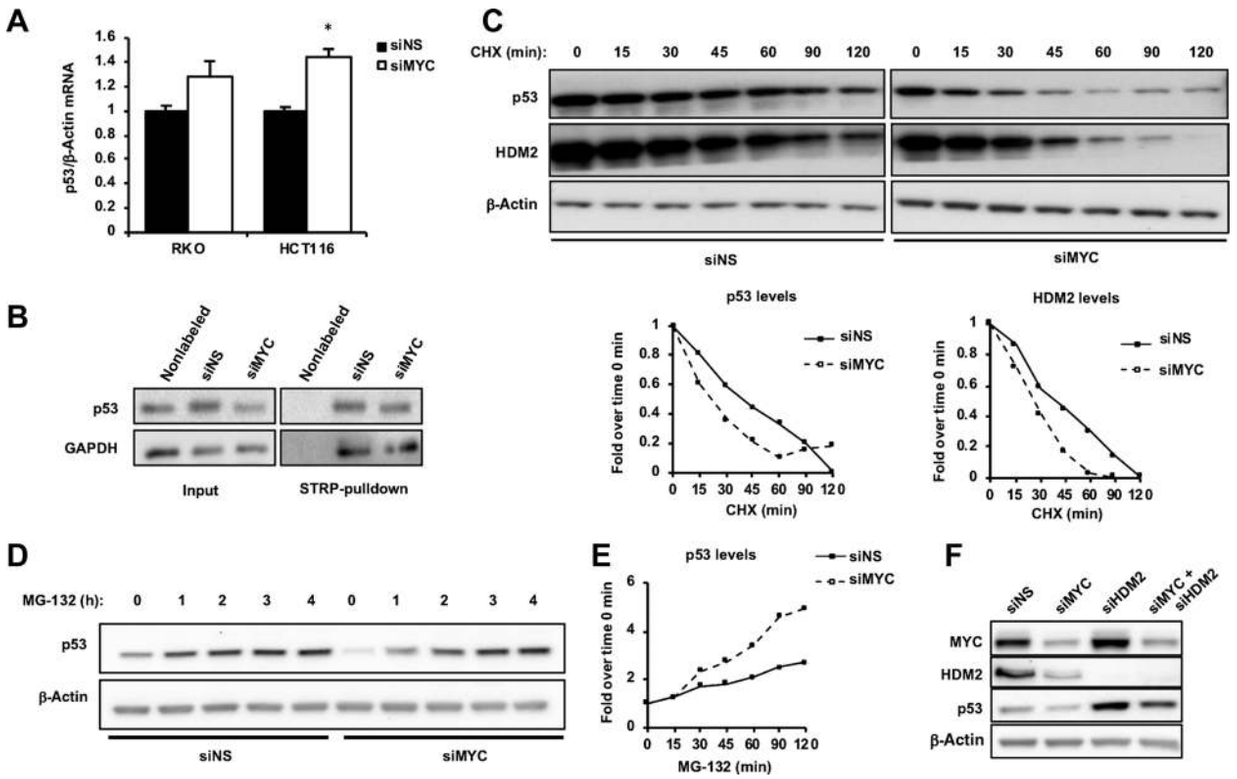

Figure 4.

Reduction of p53 protein levels is controlled at the posttranscriptional level. **A,** RKO or HCT116 cells were treated for 48 hours with siNS or siMYC. Relative *p53* mRNA levels were determined by qRT-PCR relative to *β-actin* mRNA levels (data are mean ± SEM; $n = 3$; *, $P < 0.05$ calculated by Student *t* test). **B,** p53 protein levels were analyzed as in Fig. 2D. In siMYC-treated samples, the relative values of total p53 protein and AHA-labeled nascent p53 protein, as compared with those from siNS-treated samples, were 0.48 and 0.76, respectively. **C,** After 48 hours of pretreatment with either siNS or siMYC, p53 and HDM2 protein expressions were followed in the presence of 20 μg/mL cycloheximide (CHX) for the times indicated. Western blot analyses (top plots) and relative amounts of HDM2 and p53 following normalization to β-actin (bottom plots) and considering the normalized time point 0 values as 1. **D,** Analyses of p53 protein levels in RKO cells transfected for 48 hours with either siNS or siMYC, then exposed to 10 μmol/L MG-132 for the times indicated. Western blot analyses were performed, with β-actin serving as a loading control. p53 protein values normalized to β-actin protein values in siNS- and siMYC-treated samples were 0.54 and 0.15 at time 0 and 1.39 and 1.57 at 4 hours, respectively, as quantified by densitometry. **E,** Absolute amounts of p53 protein from **D** were quantified by densitometry and normalized to β-actin protein. Relative values were obtained by setting the time point 0 values to 1. **F,** RKO cells were treated with siNS, siMYC, siHDM2, or both siMYC and siHDM2 for 48 hours, and cell extracts were examined by Western blot analysis for the indicated proteins, with β-actin serving as a loading control.

in Fig. 3C, we observed that in whole-cell extracts from *MYC* siRNA–treated cells, as compared with *NS* siRNA–treated cells, total p53 protein levels were decreasing by more than 2-fold (Fig. 4B, left). However, unlike RPL5 (Fig. 2D), the amount of newly synthesized p53 pulled down by the streptavidin beads was not as strongly affected in *MYC* versus *NS* siRNA–treated cells (Fig. 4B, right). That in MYC-depleted cells neither a reduction in *p53* mRNA levels nor p53 protein synthesis appeared to account for the strong decrease in total p53 protein levels suggested that this event may be largely mediated at the posttranslational level. To examine this possibility, we measured the half-life of p53 by Western bot analysis, as well as that of HDM2, in *MYC*-silenced RKO cells or siNS control cells, after treatment with cycloheximide. Consistent with a decrease in p53 protein stability, we found that the half-life of p53 protein and that of HDM2, in MYC depleted cells, was reduced as compared with control cells (Fig. 4C). If decreased p53 protein stability is mainly responsible for its loss in MYC-depleted cells, treatment with a proteasome inhibitor would be expected to rescue this effect. Moreover, if the levels of *p53* mRNA (Fig. 4A) and its protein synthesis are not strongly affected by MYC depletion (Fig. 4B), then such treatment should also return p53 protein to steady-state levels equivalent to those observed in *NS* siRNA–treated cells over time. When normalized to β-actin protein, the results of such an experiment show 3-fold lower levels of total p53 protein in *MYC* versus *NS* siRNA–treated cells (Fig. 4D). However, within 2 to 3 hours of posttreatment with the proteasome inhibitor MG132, total p53 protein amounts in *MYC* siRNA–depleted cells are rescued to those observed in siNS-treated cells (Fig. 4D). The enhanced rate of p53 protein degradation is readily measured by plotting its accumulation overtime (Fig. 4E). Thus, the loss of p53 protein following MYC depletion appears to be largely mediated through its degradation.

Although following MYC depletion HDM2 protein amounts in cycloheximide-treated cells continue to decline to almost undetectable levels by 120 minutes, those of p53 appeared to reach equilibrium by 60 minutes (Fig. 4C). Given that HDM2 is the major E_3 ligase for p53 and that p53 protein amounts do not fall lower after 60 minutes, whereas HDM2 protein amounts are reaching their lowest level of detection at 120 minutes, raised

the possibility that depletion of MYC led to the activation of HDM2 and the degradation of p53, as well as HDM2. By binding to the central region of HDM2, the IRBC prevents the ubiquitination of both p53 and HDM2 (27). To test whether the loss of the IRBC by MYC depletion was leading to the recovery of HDM2 activity, we treated either *NS* control cells or *MYC*-silenced cells with an siRNA directed against this E_3 ligase. The results show that depletion of HDM2 in RKO cells leads to an almost equivalent increase in p53 protein levels (Fig. 4F). Thus, the decrease in p53 and HDM2 levels following loss of MYC appears to be attributed to an increase in HDM2-mediated p53 protein degradation and HDM2 autodegradation.

MYC depletion decreases the availability of the IRBC complex

The results above demonstrate that MYC depletion in RKO cells causes a decrease in p53 protein levels due to an apparent increase in HDM2-mediated proteasomal degradation (Fig. 4E and F). Given that nascent RPs and rRNAs were decreased under conditions where MYC is depleted, raised the possibility that diminished p53 stability is regulated by a reduction in the IRBC complex. To test this possibility, we immunoprecipitated RPL5 from RKO cells treated either with *MYC* siRNA alone or *MYC* siRNA followed with actinomycin D (ActD), an inhibitor of RNA Pol I that acutely induces the IRBC (11, 13), and scored for the association of HDM2, RPL11, and *5S* rRNA in the immunoprecipitates. Prior to immunoprecipitation, cell lysates were subjected to high-speed ultracentrifugation to clear mature ribosomes, which does not alter the levels of HDM2, compared with those of the total lysates, whereas the majority of RPs are cleared from the extract (Fig. 5A). In the RPL5 immunoprecipitates from the siMYC-treated postribosomal lysates, we observe a decrease in HDM2 and RPL11 binding to RPL5 as compared with the control siNS-treated cells (Fig. 5A). Moreover, ActD treatment enhanced the binding of both HDM2 and RPL11 to RPL5 in siNS-treated control cells, and this enhanced binding was significantly reduced in MYC-depleted cells (Fig. 5A). In addition, in contrast to the RPL5 immunoprecipitates, RPL5 as well as RPL11 and HDM2 were undetectable in the IgG control immunoprecipitates from siNS control postribosomal lysates (Supplementary Fig. S3). The effects of MYC depletion in reducing the binding of HDM2 and RPL11 to RPL5 in the absence or presence of ActD were paralleled by the amounts of *5S* rRNA present in the RPL5 immunoprecipitates derived from RKO cells treated in the same manner (Fig. 5B). Taken together, the findings argue that upon MYC depletion the synthesis of the RPL5, RPL11, and *5S* rRNA is diminished, reducing the levels the IRBC complex, freeing HDM2, and allowing the degradation of p53 protein.

MYC induction leads to activation of the IRBC and increased p53

Given the findings above and those of Macias and colleagues (15) that MYC induction increases the expression of RPL5 and RPL11, the prediction would be that this would also drive increased p53 stability (15), rather than its degradation (17, 18). To test this possibility, we took advantage of U2OS cells that stably express a doxycycline-inducible MYC (22). We found that doxycycline treatment, in the presence of serum, led to a time-dependent induction of MYC, which continued to increase up to 60 hours after induction (Fig. 6A). Consistent with the findings of Macias and colleagues (15), the increases in MYC protein were paralleled by those of p53 and HDM2 (Fig. 6A). In response to activated MYC and oncogenic stress, the induction of p53 is compatible with the suppression of cell proliferation (Fig. 6B). To test the role of p53 in the proliferative response, we treated U2OS cells with a *p53* siRNA or a NS control, then induced MYC, and followed their proliferation over the next 60 hours. The results show that the p53 levels are strongly reduced under these conditions (Supplementary Fig. S4A), but unexpectedly, so was cell proliferation (Supplementary Fig. S4B). To determine if the effect of loss of p53 protein altered cell-cycle progression, we carried out a FACS analysis, which revealed a dramatic increase in tetraploid cells in the absence of p53 protein (Fig. 6C). This finding is consistent with earlier results demonstrating that depletion of p53 protein in MYC-activated cells leads to genomic instability and tetraploidy, reflecting the role of p53 in preventing DNA damage (28, 29). Thus, the data are compatible with the induction of the IRBC and p53 protein stabilization in preventing MYC-mediated oncogenic stress.

Despite the decrease in cell proliferation following MYC induction, this response is accompanied by increased levels of total RPL5 and RPL11, consistent with an increase in MYC-driven ribosome biogenesis (2). Thus, even though cell growth was declining in MYC-induced cells, the amount of ribosomes is apparently increasing. Consistent with increased ribosome biogenesis, we observed a 30% to 40% increase in ribosome production, as measured by amount of *18S* and *28S* rRNA per cell (Fig. 6D). As this increase could be attributed to aberrant expression of precursor rRNAs (30), we analyzed internal transcribed spacers of *pre-47S* rRNA (*ITS*) *1* and *2*, mature *18S* and *28S* rRNA, and a number of RPs from both ribosomal subunits. In MYC-induced cells, the results show the ITS1 and 2 are present in less than 1% of the total *18S* rRNA (Supplementary Fig. S5A), and by Northern blot analysis, there is an approximate 20% increase in mature *18S* and *28S* rRNA when comparing control and MYC-induced cells (Supplementary Fig. S5B). Roughly similar increases were observed in RPS6, RPS19, RPL26, and RPL36A, when compared with β-actin protein (see Supplementary Fig. S5C). To address whether the increase in ribosome biogenesis leads to the overexpression of ribosome-free RPL5 and RPL11, we subjected the cell lysates treated for 60 hours with doxycycline to high-speed ultracentrifugation, to clear mature ribosomes, and then analyzed the levels of free RPL5, RPL11, and HDM2. Unexpectedly, as compared with total cell extracts, there appears to be little difference in the levels of RPL5 and RPL11 in cell lysates following high-speed ultracentrifugation (Fig. 6E, left-hand plot). However, the amounts of RPL11 and HDM2 (Fig. 6E, right-hand plot), as well as those of *5S* rRNA (Fig. 6F), are dramatically enhanced in immunoprecipitates of RPL5 from doxycycline-induced MYC cells as compared with the untreated controls. Taken together, the results suggest that the induction of MYC leads to IRBC-mediated stabilization of p53 protein, and that this response is a regulated event and not due to the passive accumulation of the ribosome-free components that make up the IRBC.

Discussion

The role of MYC-mediated p53 protein regulation by RPL5 and RPL11 has been controversial (15, 17, 18). Moreover, the potential participation of *5S* rRNA in this response has not been addressed. Here, we show that the IRBC complex, which is activated in response to impaired ribosome biogenesis (2), also controls p53 protein levels in response to MYC. We found that

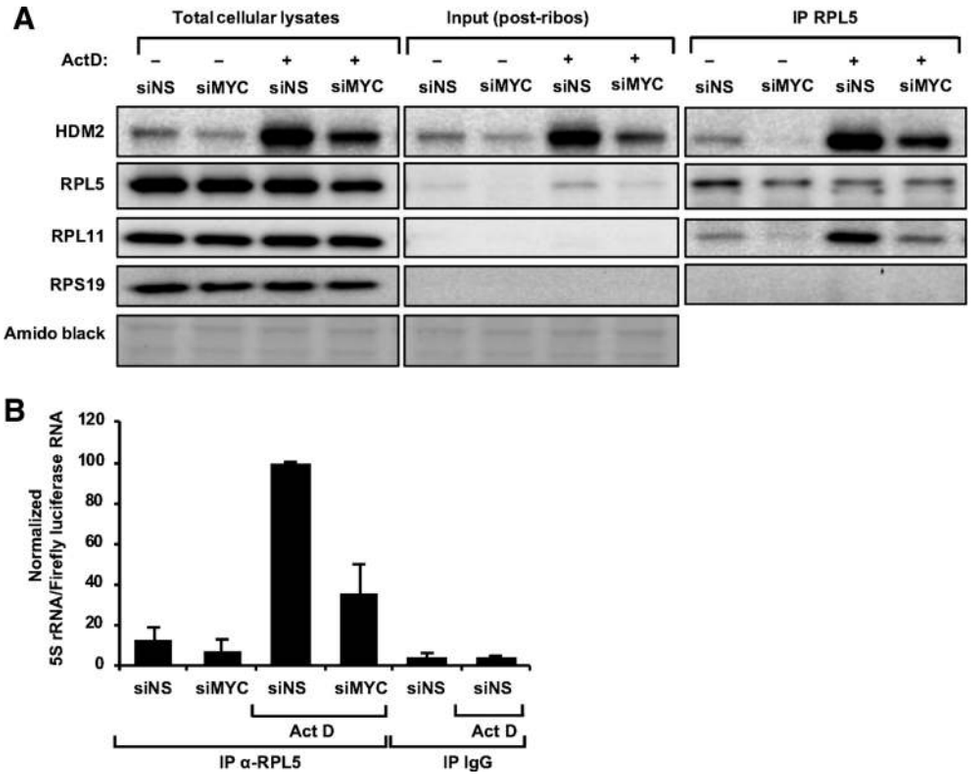

Figure 5.

Effects of depleting MYC on the IRBC complex. **A,** RKO cells were transfected for 48 hours with siNS or siMYC and then treated for 6 hours in the absence or presence of 5 nmol/L ActD. Western blot analyses show the expression levels of the indicated proteins in total cellular lysate, postribosomal lysates (Input), and immunoprecipitates from cell lysates with anti-RPL5 rabbit antibody (IP RPL5), with amido black staining serving as a loading control. **B,** RKO cells were transfected with siNS or siMYC for 48 hours and then treated in the absence or presence of 5 nmol/L ActD for 6 hrs. Cell lysates were collected, subjected to ultracentrifugation, spiked with *firefly luciferase* mRNA, and immunoprecipitated with the IgG control (IP IgG) or anti-RPL5 rabbit antibody (IP RPL5). Levels of immunoprecipitated *5S* rRNA were determined by qRT-PCR and normalized to the *firefly luciferase* mRNA. Data were normalized considering ActD-treated control from IP RPL5 as 100 (data are mean ± SEM; $n = 2$).

in colorectal cancer cell lines, when we reduce MYC levels, the amounts of the components that make up the IRBC decline, as well as those of p53 protein. We also found that, unlike previously reported (17), MYC depletion in HepG2 cells also leads to a reduction in p53 levels. Moreover, in colorectal cancer cells, we show that the loss of p53 is controlled at the posttranscriptional/posttranslational level by HDM2-mediated protein degradation, due to the apparent reduction in IRBC complexes. However, despite the diminished production of ribosomes and the components that make up the IRBC complex following MYC depletion, the IRBC is still activated following inhibition of ribosome biogenesis by ActD. In parallel, we find that MYC overexpression drives increased ribosome biogenesis, leading to oncogenic stress, the induction of p53, and a decrease in the rate of cell proliferation. Although the increase in ribosome biogenesis does not affect the levels of free RPL5 or RPL11, we find that MYC dramatically enhances the association of the IRBC complex with HDM2. This finding is consistent with the fact that the activation of the IRBC and p53 protein stabilization are not resulting from the net kinetics of the production and turnover of all of the components of the ribosome, as we have previously demonstrated by depleting cells of an essential ribosomal protein (11). Thus, in both cases, either following impairment of ribosome biogenesis or oncogene-induced hyperactivation of ribosome biogenesis, regulation of the IRBC is not a passive, but a regulated response.

Earlier studies demonstrated that RPs are overproduced and those not incorporated into preribosomes in the nucleolus are rapidly degraded in the nucleus, where they freely shuttle (8). Moreover, it is generally accepted that RP expression is largely controlled at the translational level (7). Consistent with this finding, others utilizing the same U2OS cells employed here have demonstrated that MYC controls these responses through activation of the mTOR (25). Moreover, inhibition of mTOR suppresses both the translation of the RP genes (7, 9), as well as the transcription of rRNAs, including *5S* rRNA (31). However, even though we observe an apparent inhibition in the synthesis of RPs following depletion of MYC, we find this reduction is most likely due to an apparent decrease in *RP* mRNA levels, as the proportion of *RPL5*/*RPL11* mRNAs associated with small/nonpolysomes and polysomes does not change. This mechanism of inhibition appears to be distinct from that of mTOR inhibition. The latter case is characterized by dephosphorylation of 4E-BPs and the inhibition of *5′TOP* mRNA translation, such that the *5′TOP* mRNAs accumulate in the small/nonpolysomal fraction of the sucrose gradient (9). Moreover, we recently demonstrated that

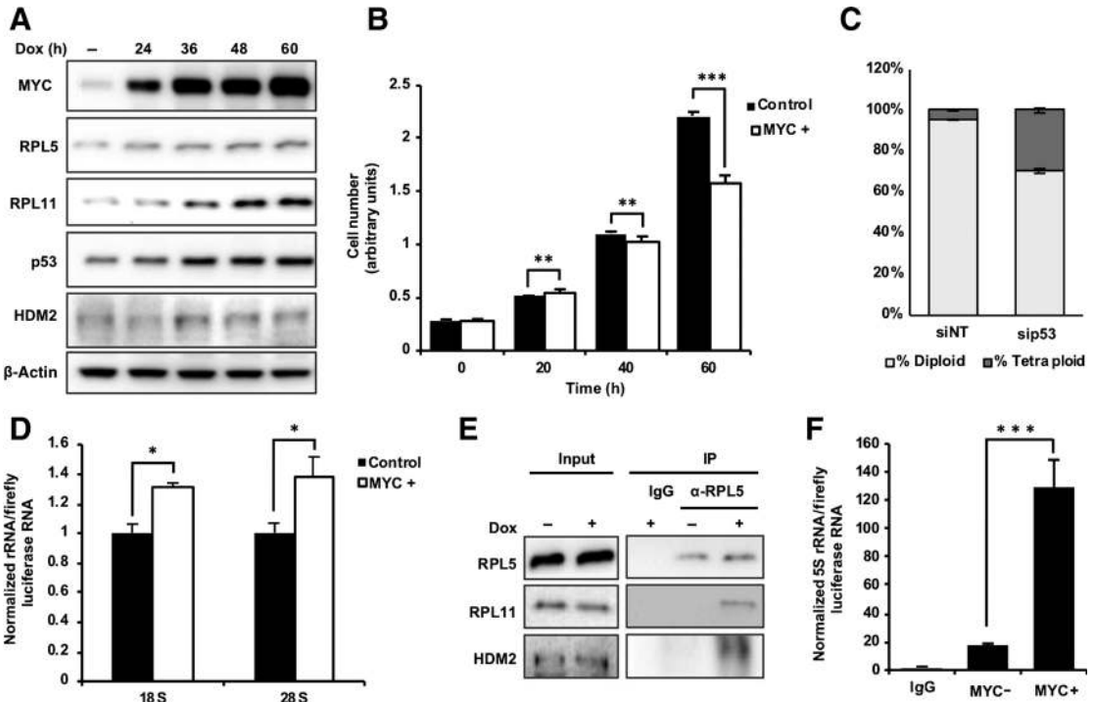

Figure 6.

Effect of MYC induction on p53 protein levels and IRBC complex formation. **A,** Following treatment for increasing time, in the presence or absence of doxycycline, total cell lysates were prepared and analyzed by Western blot for the indicated proteins. **B,** Following doxycycline treatment as in **A**, the rate of proliferation was measured by crystal violet staining (data are mean ± SEM; $n = 22$). **C,** Quantification of cell ploidy by PI-stained DNA in ethanol-fixed cells analyzed by flow cytometry as specified in Materials and Methods. Cells were transfected with either nonsilencing or *p53* siRNA and induced with doxycycline for 30 hours (data are % of total cells ± SEM; $n = 4$). **D,** Total ribosome content per cell was determined by qRT-PCR as described in Materials and Methods and normalized by spiking each sample with *firefly luciferase* mRNA (data are mean ± SEM; $n = 3$). **E,** Total lysates prepared from cells treated in the absence or presence of doxycycline for 60 hours were subjected to ultracentrifugation, and the supernatants (Input) or their immunoprecipitates (IP) were analyzed on Western blots with the indicated antibodies. **F,** Immunoprecipitates in **E** were analyzed for the presence of *5S* rRNA by qRT-PCR as described in Fig. 5B. *, $P < 0.05$; **, $P < 0.005$; ***, $P < 0.0005$, calculated by Student *t* test.

this accumulation is dependent on a complex makeup of native 40S ribosomes and the mRNA binding protein LARP1, which act to stabilize *5′TOP* mRNAs following mTOR inhibition (9). However, when we deplete MYC, we do not detect more *5′TOP* mRNAs accumulating in the nontranslated fraction of the polysome gradient, but instead we observe a general reduction of *RP* mRNAs levels, consistent with a decrease in either their transcription or their stability.

Our studies would suggest that the loss of MYC leads to a coordinate loss of *RP* mRNAs and rRNAs. Early studies showed that RPs are apparently stabilized by their interaction with rRNAs (6, 32). The reduction of *28S, 18S, 5.8S,* and *5S* rRNA synthesis observed following MYC depletion is quite severe, particularly if one considers that equal amounts of total RNA were analyzed, whereas the total amount RNA per cell is decreasing. This might suggest that loss of *5S* RNA triggers the disruption of the IRBC. However, the level of newly synthesized RPL5 is also dramatically reduced, supporting a general loss of all the components making up the IRBC. In contrast, ActD selectively inhibits Pol I–directed rRNA transcription at low concentrations and has been shown to lead to the aggregation and degradation of all RPs, except RPL11 and RPL5 (33). This is presumably due to continued synthesis of *5S* RNA by Pol III, allowing IRBC complex formation, consistent with the activation of the IRBC by ActD.

Although the enhanced association of the IRBC complex with HDM2 can be detected by either insults to ribosome biogenesis or overexpression of MYC, this appears to be a homeostatic mechanism. Recent crystallographic studies suggest that the IRBC complex interacts with HDM2 through RPL11 (34). Moreover, it has been recently proposed that during the evolution of animals, the primordial p53/HDM2 axis may have been its interaction with RPL11, allowing the cell to monitor its metabolic state through ribosome biogenesis (35). This proposal was based on the conservation of the HDM2 C305 amino acid residue and the fact that acetylation mutants of pp53, defective in inducing cell-cycle arrest and apoptosis, still regulate metabolism and retain their tumor-suppressor activity. This model is consistent with our finding that as we enhance the production of ribosomes by MYC overexpression, a cell-intrinsic mechanism mediates the activation of the IRBC leading to the stabilization of p53 protein and suppression of cell proliferation. However, the mechanism by which the preribosomal complex is redirected to the binding of HDM2 has not been resolved. It should be noted that we have previously shown that ectopic overexpressed HDM2 interacts with the IRBC complex only upon a lesion in ribosome biogenesis, indicating that an additional mechanism(s) mediates the redirection of the RPL5/RPL11/*5S* rRNA complex to HDM2 (13). Furthermore, it has been argued that it is the nascent RPL5/RPL11/

5S rRNA preribosomal complex, which is redirected to HDM2 (13, 33). This interaction appears to take place before the assembly of RPL5/RPL11/*5S* rRNA into the 90S processome, as depletion of the two catalytic components required for this event, RRS1 and BXDC1, still leads to p53 protein stabilization (13). Interestingly, in yeast, the homolog of RRS1 and BXCD1 interacts with symportin 1 (SYO1), which is required for the binding of RPL5/RPL11 with *5S* rRNA and its transport to the nucleolus and the 90S processome (36). SYO1 binds independently to RPL5 and RPL11, and in the case of RPL11, it appears to act as a chaperone until the complex is delivered to 90S processome (37). Of interest, SYO1 binds to RPL11 at the same site as HDM2, potentially placing it upstream of HDM2 in mammals. It will be important to determine whether the mammalian homolog of SYO1, HEAT repeat containing 3 (HEATR3), is implicated in the p53 protein stabilization response.

The overexpression or dysregulation of MYC has been implicated in a large number of tumor types (38). In the case of sporadic colorectal cancer, mutations in the Wnt signaling pathway, particularly the loss of tumor-suppressor adenomatous polyposis coli (*APC*), in almost all cases examined lead to elevated MYC signaling (21). First-line standard-of-care therapy for colorectal cancer is folinic acid, fluorouracil (5-FU), and oxaliplatin (FOLFOX), with folinic acid and 5-FU known to block rRNA synthesis, leading to the induction of IRBC (2). However, unexpectedly, recent studies have shown that the chief action of oxaliplatin is not to induce DNA damage, unlike other platins, but to abrogate ribosome biogenesis, leading to p53 protein stabilization (39). Moreover, this response is RPL11-dependent, and if cells are pretreated with rapamycin, which is known to block the production of the nascent IRBC complex (33), the effects of oxaliplatin are mitigated (39). These findings, added to the fact that CX5461, a Pol I inhibitor, which may have additional targets (40), blocks MYC-driven tumors in an RPL11-dependent manner (4), underscore the importance of the IRBC as a tumor suppressor.

Disclosure of Potential Conflicts of Interest

No potential conflicts of interest were disclosed.

Authors' Contributions

Conception and design: C. Morcelle, G. Thomas, A. Gentilella
Development of methodology: C. Morcelle, S. Menoyo, G. Thomas, A. Gentilella
Acquisition of data (provided animals, acquired and managed patients, provided facilities, etc.): C. Morcelle, S. Menoyo, F.D. Morón-Duran, G. Thomas
Analysis and interpretation of data (e.g., statistical analysis, biostatistics, computational analysis): C. Morcelle, F.D. Morón-Duran, S.C. Kozma, G. Thomas, A. Gentilella
Writing, review, and/or revision of the manuscript: C. Morcelle, S. Menoyo, F.D. Morón-Duran, A. Tauler, G. Thomas, A. Gentilella
Administrative, technical, or material support (i.e., reporting or organizing data, constructing databases): C. Morcelle, S. Menoyo, F.D. Morón-Duran, G. Thomas
Study supervision: G. Thomas

Acknowledgments

We thank past and present members of the Laboratory of Cancer Metabolism at IDIBELL-ICO and the Department of Internal Medicine at the University of Cincinnati for sharing ideas and reagents as well as their encouragement throughout the study. We thank M.C. Mayordomo for the preparation of figures. In addition, we thank D. Burkhart, T. Littlewood, and G. Evan for insightful discussions and M. Eilers for providing inducible MYC cells.

These studies were supported by the CERCA Program, Generalitat de Catalunya to the IDIBELL, and grants to G. Thomas and A. Gentilella from the Spanish Ministry of Economy and Competitiveness (SAF2017-84301-P), to G. Thomas from the Spanish Ministry of Economy and Competitiveness (SAF2014-52162-P), the CIG European Commission (PCIG10-GA-2011-304160), the NIH/NCI National Cancer Institute (R01-CA158768-06), the Asociación Española Contra el Cáncer (GCB-142035THOM), the ISCIII-RTICC (RD12/0036/0049), the AGAUR (2014SGR-870), and by shared funding from the IDIBELL and the Vall d'Hebron Institute of Oncology (VHIO). The Spanish Ministry grants to G. Thomas and A. Gentilella are cofunded by FEDER—a way to build Europe.

The costs of publication of this article were defrayed in part by the payment of page charges. This article must therefore be hereby marked *advertisement* in accordance with 18 U.S.C. Section 1734 solely to indicate this fact.

Received August 31, 2018; revised May 7, 2019; accepted July 3, 2019; published first July 10, 2019.

References

1. Kress TR, Sabo A, Amati B. MYC: connecting selective transcriptional control to global RNA production. Nat Rev Cancer 2015;15:593–607.
2. Pelletier J, Thomas G, Volarevic S. Ribosome biogenesis in cancer: new players and therapeutic avenues. Nat Rev Cancer 2018;18:51–63.
3. Barna M, Pusic A, Zollo O, Costa M, Kondrashov N, Rego E, et al. Suppression of Myc oncogenic activity by ribosomal protein haploinsufficiency. Nature 2008;456:971–5.
4. Bywater MJ, Poortinga G, Sanij E, Hein N, Peck A, Cullinane C, et al. Inhibition of RNA polymerase I as a therapeutic strategy to promote cancer-specific activation of p53. Cancer Cell 2012;22:51–65.
5. Granneman S, Tollervey D. Building ribosomes: even more expensive than expected? Curr Biol 2007;17:R415–7.
6. Pierandrei-Amaldi P, Beccari E, Bozzoni I, Amaldi F. Ribosomal protein production in normal and anucleolate Xenopus embryos: regulation at the posttranscriptional and translational levels. Cell 1985;42:317–23.
7. Gentilella A, Thomas G. Cancer biology: the director's cut. Nature 2012; 485:50–1.
8. Lam YW, Lamond AI, Mann M, Andersen JS. Analysis of nucleolar protein dynamics reveals the nuclear degradation of ribosomal proteins. Curr Biol 2007;17:749–60.
9. Gentilella A, Moron-Duran FD, Fuentes P, Zweig-Rocha G, Riano-Canalias F, Pelletier J, et al. Autogenous control of 5′TOP mRNA stability by 40S ribosomes. Mol Cell 2017;67:55–70e4.
10. Rubbi CP, Milner J. Disruption of the nucleolus mediates stabilization of p53 in response to DNA damage and other stresses. EMBO J 2003;22: 6068–77.
11. Fumagalli S, Di Cara A, Neb-Gulati A, Natt F, Schwemberger S, Hall J, et al. Absence of nucleolar disruption after impairment of 40S ribosome biogenesis reveals an rpL11-translation-dependent mechanism of p53 induction. Nat Cell Biol 2009;11:501–8.
12. Nicolas E, Parisot P, Pinto-Monteiro C, de Walque R, De Vleeschouwer C, Lafontaine DL. Involvement of human ribosomal proteins in nucleolar structure and p53-dependent nucleolar stress. Nat Commun 2016;7: 11390.
13. Donati G, Peddigari S, Mercer CA, Thomas G. 5S ribosomal RNA is an essential component of a nascent ribosomal precursor complex that regulates the Hdm2-p53 checkpoint. Cell Reports 2013;4: 87–98.
14. Sloan KE, Bohnsack MT, Watkins NJ. The 5S RNP couples p53 homeostasis to ribosome biogenesis and nucleolar stress. Cell Rep 2013;5: 237–47.
15. Macias E, Jin A, Deisenroth C, Bhat K, Mao H, Lindstrom MS, et al. An ARF-independent c-MYC-activated tumor suppression pathway mediated by ribosomal protein-Mdm2 interaction. Cancer Cell 2010;18:231–43.
16. Donati G, Bertoni S, Brighenti E, Vici M, Trere D, Volarevic S, et al. The balance between rRNA and ribosomal protein synthesis up- and

downregulates the tumour suppressor p53 in mammalian cells. Oncogene 2011;30:3274–88.
17. Brighenti E, Calabrese C, Liguori G, Giannone FA, Trere D, Montanaro L, et al. Interleukin 6 downregulates p53 expression and activity by stimulating ribosome biogenesis: a new pathway connecting inflammation to cancer. Oncogene 2014;33:4396–406.
18. Derenzini M, Montanaro L, Trere D. Ribosome biogenesis and cancer. Acta Histochem 2017;119:190–7.
19. Hoffman B, Liebermann DA. Apoptotic signaling by c-MYC. Oncogene 2008;27:6462–72.
20. Lowe SW, Cepero E, Evan G. Intrinsic tumour suppression. Nature 2004; 432:307–15.
21. TCGA. Comprehensive molecular characterization of human colon and rectal cancer. Nature 2012;487:330–7.
22. Walz S, Lorenzin F, Morton J, Wiese KE, von Eyss B, Herold S, et al. Activation and repression by oncogenic MYC shape tumour-specific gene expression profiles. Nature 2014;511:483–7.
23. Gentilella A, Khalili K. BAG3 expression in glioblastoma cells promotes accumulation of ubiquitinated clients in an Hsp70-dependent manner. J Biol Chem 2011;286:9205–15.
24. Boyd D, Florent G, Kim P, Brattain M. Determination of the levels of urokinase and its receptor in human colon carcinoma cell lines. Cancer Res 1988;48:3112–6.
25. Elkon R, Loayza-Puch F, Korkmaz G, Lopes R, van Breugel PC, Bleijerveld OB, et al. Myc coordinates transcription and translation to enhance transformation and suppress invasiveness. EMBO Rep 2015; 16:1723–36.
26. Haigis KM, Sweet-Cordero A. New insights into oncogenic stress. Nat Genet 2011;43:177–8.
27. Zhang Y, Lu H. Signaling to p53: ribosomal proteins find their way. Cancer Cell 2009;16:369–77.
28. Yin XY, Grove L, Datta NS, Katula K, Long MW, Prochownik EV. Inverse regulation of cyclin B1 by c-Myc and p53 and induction of tetraploidy by cyclin B1 overexpression. Cancer Res 2001;61:6487–93.
29. Yin XY, Grove L, Datta NS, Long MW, Prochownik EV. C-myc overexpression and p53 loss cooperate to promote genomic instability. Oncogene 1999;18:1177–84.
30. Kulkarni S, Dolezal JM, Wang H, Jackson L, Lu J, Frodey BP, et al. Ribosomopathy-like properties of murine and human cancers. PLoS One 2017;12:e0182705.
31. Kantidakis T, Ramsbottom BA, Birch JL, Dowding SN, White RJ. mTOR associates with TFIIIC, is found at tRNA and 5S rRNA genes, and targets their repressor Maf1. Proc Natl Acad Sci U S A 2010;107:11823–8.
32. Warner JR. In the absence of ribosomal RNA synthesis, the ribosomal proteins of HeLa cells are synthesized normally and degraded rapidly. J Mol Biol 1977;115:315–33.
33. Bursac S, Brdovcak MC, Pfannkuchen M, Orsolic I, Golomb L, Zhu Y, et al. Mutual protection of ribosomal proteins L5 and L11 from degradation is essential for p53 activation upon ribosomal biogenesis stress. Proc Natl Acad Sci U S A 2012;109:20467–72.
34. Zheng J, Lang Y, Zhang Q, Cui D, Sun H, Jiang L, et al. Structure of human MDM2 complexed with RPL11 reveals the molecular basis of p53 activation. Genes Dev 2015;29:1524–34.
35. Lane DP, Verma C. Mdm2 in evolution. Genes Cancer 2012;3:320–4.
36. Kressler D, Bange G, Ogawa Y, Stjepanovic G, Bradatsch B, Pratte D, et al. Synchronizing nuclear import of ribosomal proteins with ribosome assembly. Science 2012;338:666–71.
37. Calvino FR, Kharde S, Ori A, Hendricks A, Wild K, Kressler D, et al. Symportin 1 chaperones 5S RNP assembly during ribosome biogenesis by occupying an essential rRNA-binding site. Nat Commun 2015;6: 6510.
38. Dang C. MYC on the path to cancer. Cell 2012;149:22–35.
39. Bruno PM, Liu Y, Park GY, Murai J, Koch CE, Eisen TJ, et al. A subset of platinum-containing chemotherapeutic agents kills cells by inducing ribosome biogenesis stress. Nat Med 2017;23:461–71.
40. Xu H, Di Antonio M, McKinney S, Mathew V, Ho B, O'Neil NJ, et al. CX-5461 is a DNA G-quadruplex stabilizer with selective lethality in BRCA1/2 deficient tumours. Nat Commun 2017;8:14432.